A Planar Variable Reluctance Magnetic Micromotor With Fully Integrated Stator And Wrapped Coils

Chong H. Ahn, Yong J. Kim, and Mark G. Allen
School of Electrical Engineering
Microelectronics Research Center
Georgia Institute of Technology
Atlanta, GA 30332-0250

ABSTRACT

A new, fully functional, electrically excited planar variable reluctance magnetic micromotor has been demonstrated on a silicon wafer. The motor uses a micromachined nickel-iron rotor and a fully integrated stator, in which a new toroidal-meander type integrated inductive component is used for flux generation. To reduce the magnetic reluctance in the stator, a modified stator geometry was adopted which removes the yoke which is used in a conventional reluctance motor. Using polyimide as both an integral structural material and as an electroplating mold, a 40 μm thick nickel-iron rotor 500 μm in diameter was micro-assembled onto a fully integrated nickel-iron stator 120 μm in thickness. When 500 mA of current was applied to each stator, 12° of rotation (1 stroke in this motor) was observed. By applying three phase 200 mA current pulses to the stators, rotation of the rotor was observed. The speed and direction of the rotation could be adjusted by changing the frequency and phase firing order of the power supply respectively. Continuous rotor rotation was observed at speeds up to 500 rpm; this speed limitation was solely due to the limitation of the maximum frequency of the controller used. The predicted torque for the fabricated micromotor at 500 mA driving current was calculated to be 1.2 (μN-m).

INTRODUCTION

Recently there has been much work towards realizing practical micromotors using different operating principles for a variety of applications. These efforts have focused mainly on electrostatic drive [1,2], but ultrasonic [3], dielectric induction [4], and magnetic drives [5,6] have also been investigated. Among several proposed operating principles, magnetic micromotors are attractive in applications such as conductive fluids for some biomedical applications, and operation in environments where high driving voltages are unacceptable or unattainable.

In realizing a magnetic-based micromotor, hybrid techniques have been used to either place permanent magnet components onto integrated planar coils [5] or to introduce external magnetic fields onto integrated high-permeability moving parts [6]. One reason that these approaches have been taken is due to the difficulty in fabricating three dimensional 'wrapped' coils using an integrated, planar fabrication process. However, recently a new planar integrated meander inductive component was proposed and demonstrated [7], in which multilevel magnetic cores were 'wrapped' around planar meander conductors. This configuration can be thought of as the result of interchanging the roles of the conductor wire and magnetic core in a conventional inductor. A schematic drawing of a section of the integrated toroidal-meander type inductor is shown in Figure 1. With this integrated inductive

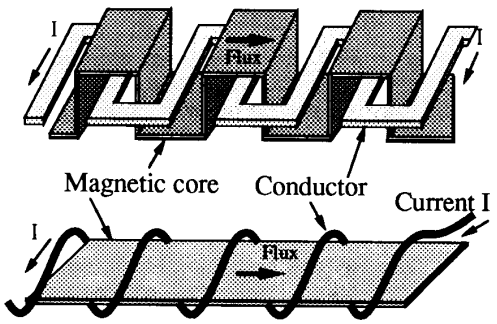

Figure 1. Meander type inductive component (top). A multilevel magnetic core is 'wrapped' around a planar conductor coil. This structure is analogous to the more familiar standard inductive component (bottom)

component, it is possible to guide magnetic flux confined in an integrated magnetic core to the locations where magnetic actuation or sensing take place. Thus, this integrated inductive component makes it possible to fabricate a magnetic microactuator in a fully integrated fashion; such a device using a movable cantilever beam has recently been demonstrated [8]. Using this component as the basis for a micromotor stator to generate magnetic flux, a new fully functional, electrically excited planar variable reluctance magnetic micromotor has been demonstrated on a silicon wafer. This motor has a similar operating principle to the conventional magnetic variable reluctance motor. For a preliminary demonstration, stators (with fully integrated coils) and rotors are fabricated separately, and then assembled together using microassembling techniques [9], although the process used for fabrication is completely compatible with fully integrated devices.

MOTOR DESIGN

A variable reluctance magnetic motor has two sets of salient poles, one set in the stator (which usually has excitation coils wrapped around the magnetic poles) and another set on the rotor. This motor requires no permanent magnets to produce a torque moment. The stator coils arranged in one or more sets and phases should be excited individually or in pairs to produce torque for rotor rotation. When a phase coil is excited, the nearest rotor poles that are located to the excited stator poles are attracted to the stator poles. Due to the rotation of the rotor, when the rotor poles are aligned with the excited stator poles, the excited phase should be off and the next phase is then excited to maintain continuous rotor rotation.

0-7803-0957-2/93 $3.00 © 1993 IEEE

A conventional variable reluctance magnetic motor as shown in Figure 2(a) consists of the rotor and the stator, whose stator always contains magnetic yokes to form a magnetic path from one stator pole, through the rotor, through the stator pole directly across from the first pole, and back around the yoke to the first pole. This works well in conventional motors since the reluctance of the yoke can usually be neglected. However, in contrast to conventional magnetic circuits, a micromachined magnetic circuit usually has a high magnetic reluctance due to processing limitations on the achievable permeability of the magnetic core. In fact, in many micromagnetic actuators, the reluctances of the core and air gap can be comparable [8]. Thus, reduction of the core reluctance is a major concern in realizing a micromachined magnetic circuit. If the permeability cannot be increased, the geometry must be modified. The major geometric factors which affect the reluctance in a magnetic core are the magnetic core area and length. Since the magnetic core area is limited by planar geometric constraints, one of the best design strategies to reduce the magnetic reluctance is to shorten the length of the magnetic core.

This motivation to minimize core reluctance makes it desirable to modify the standard variable reluctance motor design [10], since the long magnetic path through the yoke adds significantly to the core reluctance. A schematic diagram of the modified design is shown in Figure 2(b). The wound poles of all phases are arranged in pairs of opposite polarity to achieve adjacent pole paths of short lengths. The stator poles are positioned so as to greatly shorten the magnetic flux paths and to provide an isolated magnetic core for the flux path of each phase. This isolated magnetic circuit reduces both 50% of the core reluctance and 40% of the core loss [10]. In addition, it is possible to wind coils on the outside of the core, which increases both the number of turns which can be achieved as well as allowing the bonding pads to be on the periphery of the motor.

The poles are wound oppositely in pairs to form the phases, then each phase produces a pulse of torque on each passing rotor pole. The fundamental switching frequency to rotate a rotor with a speed n (rev/sec) is

$$f = nN_r \qquad (1)$$

where N_r is the number of rotor poles.

If a motor has q phases, qN_r steps are required per revolution, where the 'stroke' (or 'step angle') is

$$S = \frac{2\pi}{qN_r}\ (rad). \qquad (2)$$

The designed magnetic micromotor with no external yoke has 12 stator poles and 10 rotor poles (12/10) in 3 phases (as opposed to a conventional 12/8(stator/rotor) design) and it has 12° of rotation in one stroke. Two stator pole pairs in the same phase are located in the opposite direction through rotor poles, where each stator pole pair contains 7 turns of toroidal-meander coil. The angle between rotor poles is 36°, the stator angles are 36° / 24 °, and the required strokes per revolution is 30. Table I shows a list of other feasible pole arrangements for this type of motor design.

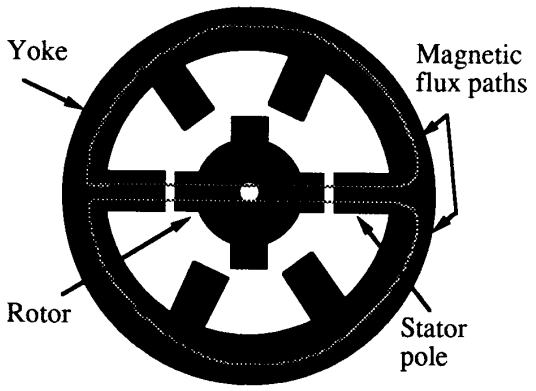

(a)

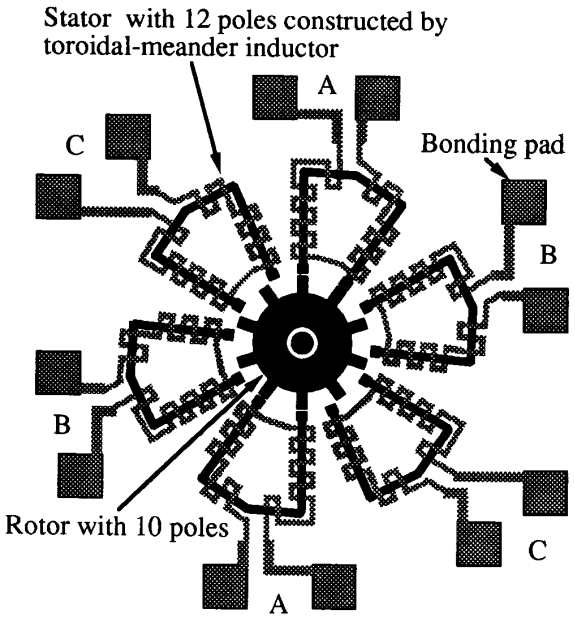

(b)

Figure 2. Structure of conventional and modified variable reluctance motors. (a) Schematic diagram of the magnetic core of a conventional magnetic variable reluctance motor showing the yoke frame. (b) Schematic diagram of modified planar variable reluctance magnetic motor fabricated in this work. The structure consists of 12 stator poles and 10 rotor poles in three phases. Each magnetic core is separated from the others.

Table I. Some Possible Rotor/Stator Pole Combinations for Motor Shown in Fig. 2(b)

Number of phases	Stator/ rotor poles	Strokes per rotation	Rotor angle (degree)	Stator angles (degree)
2	4/3	6	120	120/60
3	6/5	15	72	72/48
3	12/10	30	36	36/24
4	16/14	48	25.7	25.7/38.6
5	10/9	45	40	40/32

FABRICATION

The stator and pin were fabricated using a polyimide multilevel metal interconnection technique, in which an electroplated high permeability nickel(81%)-iron(19%) magnetic core was used as the magnetic material.

A brief fabrication process of this micromotor is shown in Fig. 3. The process starts with 3-inch <100> silicon wafers as a substrate, onto which was deposited 0.6 μm of PECVD silicon nitride. Onto this substrate, chromium (500 Å) / copper (2000 Å) / chromium (700 Å) layers were deposited using electron-beam evaporation to form an electroplating seed layer. Polyimide (Dupont PI-2611) was then spun on the wafer in multiple coats to build electroplating molds for the bottom magnetic core. Four coats were used to obtain a 40 μm thick polyimide film. Each coat was cast by continuous two-step spin speeds; 700 rpm for 10 seconds and then 3000 rpm for 4 seconds, and soft baked for 10 minutes at 120 °C prior to the application of the next coat. After deposition of all coats, the polyimide was cured at 350 °C for 1 hour in nitrogen, yielding an after-cure thickness of 40 μm. Holes which contain bottom magnetic cores were etched in this polyimide using a 5% CF_4/O_2 plasma etch and an aluminum hard mask until the chrome/copper/chrome seed layer was exposed. The electroplating forms were then filled with nickel (81%) - iron (19%) permalloy using standard electroplating techniques [11] and the nickel-iron electroplating bath described in Table II. To electroplate the bottom magnetic cores, electrical contact was made to the seed layer, and the wafers were immersed in the plating solution. During the electroplating, the solution was maintained at room temperature and a pH of approximately 2.7, and was stirred very slowly with a Teflon propeller blade. An applied current density of 2 mA/cm^2 resulted in a electroplating rate of 0.1-0.15 μm/minute. In order to insulate the bottom magnetic core from the conductor coil, polyimide was spin-coated (as above) with two step speeds and hard-cured at 350 °C for 1 hour. To construct a thick planar meander conductor coil, copper was plated through a thick photoresist mold. A chromium (500 Å) / copper (2000 Å) / chromium (700 Å) seed layer was deposited, and a 60 μm wide copper plating mold was formed in 8 μm thick positive photoresist. The copper conductors were plated through the defined molds using standard electroplating techniques and the copper plating solution described in Table II. To facilitate gold wire bonding for the final test, 0.5 μm thick gold was plated on the top of plated copper conductor coils and bonding pads using a commercial cyanide-based gold plating bath. The measured resistance of conductor coil per stator was approximately 1.5 ohms. Note that the bottom magnetic core is electrically isolated from the plating solution during this step. Upon completion of the electroplating, the photoresist was removed with acetone, and the copper seed layer was etched in an sulfuric-acid-based copper etching solution.

In order to insulate the conductor line and re-planarize the surface, one coat of polyimide approximately 10 μm in thickness was deposited and cured as described above. Via holes were then dry-etched through the polyimide layer between the meander conductors using 100% oxygen plasma and an aluminum hard mask. Upon completion of the via etch, the aluminum hard mask was removed. Because the bottom magnetic core was exposed to the oxygen plasma

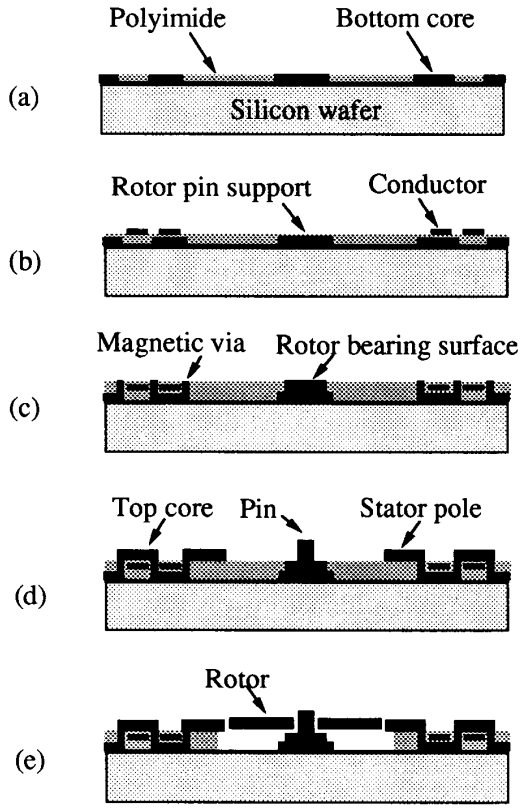

Figure 3. Fabrication sequence for the magnetic micromotor. (a) polyimide deposition, dry etching, and bottom core electroplating; (b) patterning of conductor; (c) magnetic via and rotor pin electroplating; (d) top core and stator pole electroplating; (e) rotor and stator microassembly.

Table II. Nickel-iron and copper electroplating bath compositions.

Nickel-iron		Copper	
Component	Quantity(g/l)	Component	Quantity
$NiSO_4.6H_2O$	200	$CuSO_4.5H_2O$	1200 (g/l)
$FeSO_4.7H_2O$	8	H_2SO_4	100 (ml/l)
$NiCl_2.6H_2O$	5		
H_3BO_3	25		
Saccharin	3		

during dry etching, the surface of magnetic core was oxidized. To remove the oxide film, the exposed areas of the bottom magnetic cores were etched in a 2% hydrofluoric acid solution for 30 seconds. Contact was then made to the bottom magnetic core, and the vias were filled with nickel-iron using the electroplating bath and conditions described previously. Upon completion of the via electroplating, an evaporated nickel seed layer was defined between the magnetic vias using a liftoff technique for the electroplated top cores. A 1000 Å chromium layer was then deposited as a dummy seed layer to provide an uniform magnetic top core plating and to protect the defined nickel seed layer. Stator poles, rotor pins, and top magnetic cores were processed on the same level, which requires high aspect ratio structures. In order to obtain high

aspect ratio patterns, photosensitive polyimide 40 μm in thickness was used as a plating mold for the top patterns of both stators and rotors. Photosensitive polyimide processing [9] has already been demonstrated to construct 100 μm high structure with a high aspect ratio of 8 (structure height/width) using conventional photolithography techniques. Plating molds 40 μm in depth were obtained using a photosensitive polyimide (Ciba-Geigy probimide 349), and top magnetic cores and structures were then plated after removing the chromium layer on the bottom of plating molds. Upon completion of the top core electroplating, the photosensitive polyimide and chromium seed layer were removed. The final thickness of the stator relative to the substrate is approximately 120 μm. Bonding pads were then opened in the polyimide layers by using the via etch process sequence described earlier. Optionally, to remove the chrome / copper / chrome plating seed layer located underneath the polyimide, the structure was dry etched to the bottom, and the chrome/copper/chrome was then selectively wet etched. It should be noted that removal of the magnetic core plating base was not required for successful device performance (this is a benefit of the meander inductor geometry). In a separate process, 40 μm thick nickel-iron rotors 600 μm in diameter were plated separately using the same photosensitive process described earlier and a chromium (500 Å) / copper (1 μm) /chromium (700 Å) sacrificial seed layer. These rotors were released from the substrate and assembled with stators. Figure 4 shows a photomicrograph of the assembled planar variable reluctance magnetic micromotor, the outer stator diameter of which is 1.5 mm. Upon completion of the fabrication, samples were diced and bonded for test.

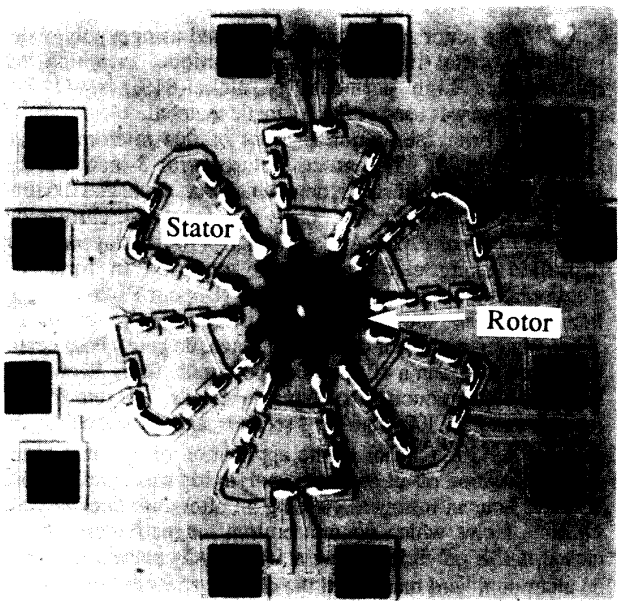

Figure 4. Photomicrograph of the fully fabricated micromotor.

THEORY

When current is applied to the phase winding, the rotor tends to align with the stator poles. A torque is produced to move the rotor to a minimum-reluctance position. The inductance L will be varied between minimum and maximum values as the rotor rotates.

The maximum inductance occurs when the rotor and stator poles are aligned and the minimum inductance occurs when a rotor interpolar axis is aligned with the stator poles, thus the inductance $L(\theta)$ changes with instantaneous rotor position θ. If it is assumed that magnetic saturation is negligible and the linear relationship between flux-linkage and driving current is valid at the instantaneous rotor position θ, the produced torque at the rotor is

$$T = \frac{1}{2} i^2 \frac{dL(\theta)}{d\theta}, \qquad (3)$$

where i is the applied current to the stator coil.

A rough estimate of the maximum attainable torque was derived using an idealized maximum available energy conversion in energy conversion loop by Harris[12] as

$$T = (vol)\frac{N_r B_s^2 (\lambda - 1) q \beta g}{2\pi \mu_0 r_1} \text{(N-m)}, \qquad (4)$$

where (vol) is the rotor volume; B_s is the magnetic flux density in the stator poles at the maximum flux linkage in the aligned position; λ is the aligned/unaligned unsaturated inductance ratio; β is the pole arc (assumed stator and rotor have the same arc); g is the air gap.

In the fabricated micromotor as shown Figure 4, the inductance ratio (aligned/unaligned) λ is approximately 9 assuming an air gap of 5 μm. Assuming a relative permeability μ_r of 500 [8], and a saturation flux density of 0.8 (T) [8], the predicted torque was estimated as 1.2 (μN-m) for a stator current of 500 mA.

EXPERIMENTAL RESULTS

The measured resistance of a single coil was approximately 1.5 ohms. A test of the maximum current that these coils could withstand was performed. Continuous currents of between 2.5 and 3 amperes could be sustained continuously. Coil failure was not observed until continuous current reached over 4 amperes.

The first test of micromotor operation was to observe stepping action as phases were sequentially excited. Figure 5 shows the result of this experiment. In Figure 5(a), the rotor is shown in a position which is misaligned in comparison to the phase which is to be activated. Upon application of 500 mA to the active phase, rotational actuation was observed as shown in Figure 5(b). The rotor has aligned exactly to the active phase as predicted. This experiment shows that the motor is working well.

The next test of operation was to sustain a continuous rotation of the rotor. The simple excitation apparatus used to drive the fabricated micromotor is described below. A standard curve tracer was used as a DC power source in order to protect the micromotor under test by limiting the maximum power dissipation. A mechanical rotary switch

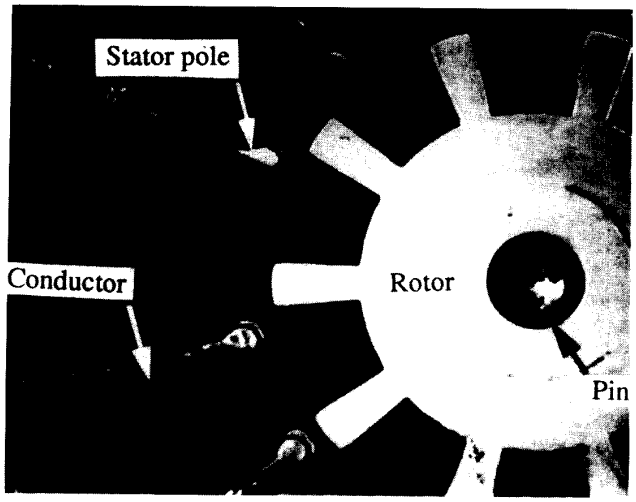

(a)

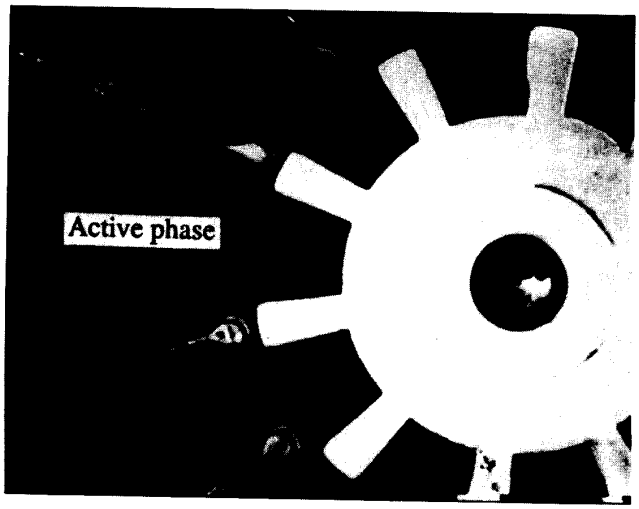

(b)

Figure 5. Photomicrograph of the actuated rotor. When 500 mA of current was applied to each stator phase, 12 ° of rotation (1 stroke in this motor) was observed. (a) before current is applied; (b) after current is applied, rotor poles are aligned to the stator poles of the active phase.

driven by a variable speed AC motor was used to generate a three phase DC square wave. The frequency of the three phase square waves could be adjusted by varying the speed of the AC motor, thus controlling the rotation speed of the micromotor under test.

The three phase square waves generated from the rotary switch were then applied to the corresponding stator windings. Pole pairs in the same phase were connected so as to minimize the path length of the magnetic flux in the rotor. Applied currents of 300-500 mA with a driving voltage less than 1 (V) were sufficient to initiate motion from rest. By changing the rotation direction of the AC motor keeping the micromotor connections constant or by exchanging two of the phase connections of the micromotor keeping the rotation direction of AC motor constant, the rotation direction of the magnetic micromotor could be changed reversibly.

Although the maximum frequency of the driving pulse (and therefore the maximum micromotor speed) was limited by the mechanical rotary switch, the micromotor could be reproducibly started, stopped, reversed, and continuously rotated at speeds up to 500 rpm. It is fully expected that using electronic motor drive controllers, speeds in the thousands of rpm will be attainable. Such drive electronics are currently under development.

CONCLUSIONS

A new planar variable reluctance magnetic micromotor has been demonstrated on a silicon wafer with a micromachined nickel-iron rotor and a fully integrated stator, in which a new meander type integrated inductive component has been used as the basic component for stator flux generation. A modified geometry from the conventional variable reluctance motor was utilized in order to minimize core reluctance. When 500 mA of current with a driving voltage less than 1 (V) was applied to each stator, 12° of rotation (1 stroke in this motor) was observed. The micromotor could be reproducibly started, stopped, reversed, and continuously rotated at speeds up to 500 rpm. The rotation speed was limited to 500 rpm by the driving controller used. Drive electronics capable of higher speeds are currently under development. The predicted torque for the fabricated micromotor at 500 mA drive current was equal to 1.2 (μN-m).

ACKNOWLEDGEMENT

This work was supported in part by the National Science Foundation under grant ECS-9117074. The authors would like to thank Mr. Young W. Kim, Mr. Jeong B. Lee, and Mr. Bizhan Rashidian for valuable technical discussions, Mr. Robert Carnahan for the mask fabrication, and in particular Mr. A. Bruno Fraizer for his tremendous support on the photosensitive polyimide processing. Microfabrication was carried out at the Georgia Institute of Technology Microelectronics Research Center (MiRC). The authors wish to thank the MiRC staff for their assistance. The authors would also like to gratefully acknowledge DuPont and Ciba-Geigy for their donation of regular and photosensitive polyimides which have been used in this work.

REFERENCES

[1] L. S. Fan, Y. C. Tai, and R. S. Muller, "IC-processed electrostatic micromotors", Sensors and Actuators, Vol. 20, pp. 41-47, 1989.

[2] M. Meheregany, P. Nagarkar, S. D. Senturia, and J. H. Lang, "Operation of microfabricated harmonic and ordinary side-drive motors", Proc. 3rd IEEE Workshop on Micro Electro Mechanical Systems, pp. 1-8, Napa Valley, CA, Feb. 1990.

[3] K. R. Udayakumar, S. F. Bart, A. M. Flynn, J. Chen, L. S. Tavrow, L. E. Cross, R. A. Brooks, and D. J. Ehrlich, "Ferroelectric thin film ultrasonic micromotor", Proc. 4th IEEE Workshop on Micro Electro Mechanical Systems, pp.

109-113, Nara, Japan, 1991.

[4] S. F. Bart and J. H. Lang, "An analysis of electro-quasistatic induction micromotors", Sensors and Actuators, Vol. 20, pp. 97-106, 1989.

[5] B. Wagner, M. Kreutzer, and W. Benecke, "Linear and rotational magnetic micromotors fabricated using silicon technology", Proc. IEEE Microelectromechanical Systems Workshop, pp. 183-189, 1992.

[6] H. Guckel and K. J. Skrobis and T. R. Christenson and J. Klein and S. Han, B. Choi and E. G. Novell and T. W. Chapman, "On the application of deep X-ray lithography with sacrificial layers to sensor and actuator construction(The magnetic micromotor with power takeoffs)", Proc. Transducers '91, 6th International Conference on Solid-State Sensors and Actuators, Late News, San Francisco, CA, June, 1991.

[7] C. H. Ahn and M. G. Allen, "A new toroidal-meander type integrated inductor with a multilevel meander magnetic core", submitted to IEEE Trans. on Magnetics.

[8] C. H. Ahn and M. G. Allen, "A fully integrated micromagnetic actuator with a multilevel magnetic core", Digest, IEEE Solid State Sensor and Actuator Workshop, PP. 14-18, Hilton Head, SC, June 1992.

[9] A. B. Frazier and M. G. Allen, "High aspect ratio electroplated microstructures using a photosensitive polyimide process", Proc. IEEE Microelectromechanical Systems Conference, pp. 87-92, Germany, Feb. 1992.

[10] J. R. Hendershot, Jr., "Switched reluctance brushless DC motor with low loss magnetic circuits ", Proc. Sixteenth International Intelligence Motion Conference, Long Beach, CA, U.S.A., 1989.

[11] I. W. Wolf, "Electrodeposition of magnetic materials", Journal of Applied Physics, Vol. 33, No. 3, pp. 1152-1159, Mar. 1962.

[12] M. R. Harris, "Static torque production in saturated doubly-salient machines", Proc. IEE, Vol. 122, pp. 1121-1127, 1975.

[13] T. J. E. Miller, Brushless Permanent-Magnet and Reluctance Motor Drives, Clarendon Press Oxford, New York, 1989.